ELSEVIER

Contents lists available at ScienceDirect

Journal of Hydrology

journal homepage: www.elsevier.com/locate/jhydrol



Research papers



Contrasting stream water temperature responses to global change in the Mid-Atlantic Region of the United States: A process-based modeling study

Yuanzhi Yao ^a, Hanqin Tian ^{a,*}, Latif Kalin ^a, Shufen Pan ^a, Marjorie A.M. Friedrichs ^b, Jing Wang ^{a,c}, Ya Li ^{a,d,e}

- a International Center for Climate and Global Change Research, School of Forestry and Wildlife Sciences, Auburn University, Auburn, AL 36832, USA
- ^b Virginia Institute of Marine Science, William & Mary, Gloucester Point, VA, USA
- c State key Laboratory of Urban and Regional Ecology, Research Center for Eco-Environmental Sciences, Chinese Academy of Sciences, Beijing 100085, China
- d Research Center for Eco-Research Center for Eco-Environmental Science, Chinese Academy of Science, Beijing 100085, China
- e University of Chinese Academy of Sciences, Beijing 10049, China

ARTICLE INFO

This manuscript was handled by Marco Borga, Editor-in-Chief

Keywords:
Dynamic Land Ecosystem Model (DLEM)
Global change
Mid-Atlantic Region
Stream order
Water temperature

ABSTRACT

The accurate estimation of stream water temperature is essential for understanding environmental controls on the structure and functioning of aquatic ecosystems. Few studies have coupled soil and stream water temperatures to capture the synergy of thermal balances between terrestrial and riverine systems. As a result, little is known about how multiple environmental stresses have affected water temperature, particularly for different orders of streams. Here we incorporated a new water transport scheme into the Dynamic Land Ecosystem Model (DLEM) to predict water temperature in 1st order and higher-order streams (>1st order). Driven by a 4-km georeferenced dataset of multiple environmental factors, our new water temperature model was utilized to predict the spatiotemporal variations of water temperature in the U.S. Mid-Atlantic Region during 1900-2015. Results revealed that water temperature during 1970–2015 increased significantly (p < 0.05), and the rate of increase of the 1st order streams 0.32 °C•decade⁻¹ is higher than that of higher-order streams 0.28 °C • decade ⁻¹. The buffering effect of groundwater on water temperature in 1st order streams diminished under the context of climate warming. Factorial analysis showed that climate change and variability explain most of the changes (~80%) in stream water temperature since 1900. Land-use conversions (mostly from cropland to forest), CO2 fertilization, and land nitrogen management collectively explained a greater percent of change in water temperature in 1st order streams (24%) than higher-order streams (9%), implying that 1st order streams are particularly vulnerable to human activities.

1. Introduction

Stream water temperature is a fundamental physical variable reflecting the balance of thermal energy in aquatic systems (Chapra, 2008). It has been well documented that stream water temperature can substantially affect the solubility of oxygen and other gases (Sander, 2015), govern the decomposition or mineralization rate of organic matter (Pastor et al., 2003), and regulate the fate of nitrogen (Harrison et al., 2009) and phosphorus (McQueen and Lean, 1987). Water temperature also moderates the metabolic rate of microorganisms (Claireaux et al., 2000) and can shape the spatial distribution of habitats supporting aquatic species (Isaak et al., 2010). Given its importance to aquatic biogeochemistry and biodiversity, significant efforts have been

devoted to monitoring and estimation of water temperature (Van Vliet et al., 2013).

Although ubiquitous water discharge monitoring sites have been established worldwide, water temperature observations are still lacking (Wanders et al., 2019). A modeling approach is needed to construct the spatial and temporal patterns of stream water temperature across large regions. Empirical relationships, derived from the regression analysis of observed water temperature and air temperature, are commonly deployed in water quality models due to their relative simplicity (Leach and Moore, 2019). Such relationships can provide reliable estimates of water temperature for regional studies because the regression parameters can be calibrated to match the data. As a result, the performance of an empirically based model strongly depends on the amount and quality

E-mail address: tianhan@auburn.edu (H. Tian).

^{*} Corresponding author.

of data from the study region. If the environmental conditions change, the skill of these models in predicting water temperature may drop (Arismendi et al., 2014). The reason for this is that empirical relationships cannot represent the mechanisms of how environmental factors contribute to changes in stream water temperature. This inherent weakness has hampered their application in long-term studies where land use and land management change over time.

Stream water temperature is highly sensitive to climate change and anthropogenic disturbances. For instance, water temperature has been increasing in streams draining to the Chesapeake Bay, USA, which aligns with the increase in air temperature in the region (Rice and Jastram, 2015). Land management, such as forest clear-cutting, can also significantly impact water temperature (Chen et al., 2016; Brown and Krygier, 1970). Management of water resources, such as dam construction or reservoir operations, can cool or warm water temperature under different environmental conditions due to the changes in water surface area and the thermal energy leaking from the bottom of the reservoirs (Chen & Fang, 2015b).

In recent years an improved understanding of the energy balance in streams has been obtained through field studies, which has subsequently promoted the development of physically-based approaches that incorporate climate and hydraulic variables into the energy balance equations. These models have found applications at the basin level (Wu et al., 2012), regional level (Buccola et al., 2016; Isaak et al., 2017), continental level (Li et al., 2015b), and global level (Van Vliet et al., 2013; Wanders et al., 2019). Physically-based models can capture the changes in environmental conditions and provide reliable results for historical data reconstruction (Wanders et al., 2019) and future projections (Ficklin et al., 2014; Wu et al., 2012). However, physically-based models still need certain assumptions to simplify the processes that are not understood well or are too complex. Therefore, empirical equations are commonly incorporated into physically-based models to estimate water temperature of 1st order streams, often as a boundary condition (Haag and Luce, 2008; Van Vliet et al., 2012).

To the best of our knowledge, few studies presented the spatial distribution of stream temperature in headwaters over a large region. The headwater zone, known as the terrestrial-aquatic interface, has been recognized as a hotspot for greenhouse gas (GHG) emissions (Butman and Raymond, 2011) and has therefore prompted significant interest from both field research and modeling communities. For example, a recent study has suggested that headwater streams can be important refuges for cold-water species under the risk of changing climate (Isaak et al., 2016). Although this study suggested that headwater zones can buffer the impact of climate (small headwater streams have cooler water temperature in summer and warmer water temperature in winter than higher-order streams), they are particularly vulnerable to climate change and human activities, especially when environmental change reaches a tipping point (Nepstad et al., 2008). Over the past century, headwater zones have been heavily impacted by human and/or natural disturbances (Isaak et al., 2010; Cover et al., 2010). For example, some studies have found ~5 °C increase in water temperature of headwater streams after fire disturbances, suggesting a strong synergy between land surface processes and water temperature (Isaak et al., 2010; Koontz et al., 2018).

In this study, we coupled a new water transport scheme, called Model for Scale Adaptive River Transport (MOSART) (Li et al., 2013; Li et al., 2015b) with our land ecosystem model (Dynamic Land Ecosystem Model, DLEM) (Tian et al., 2015). We incorporated a physically-based water temperature model into DLEM. We linked a simplified groundwater process to the stream water as a boundary condition and improved the model representation of the groundwater-fed, sub-grid routing thermal energy exchanges within the 1st order streams. The objectives of this study are to (1) evaluate the spatial and temporal patterns of water temperature of head water streams and higher-order (>1st order) streams from 1900 to 2015 across the Mid-Atlantic region (including the Chesapeake Bay and Delaware Bay Watersheds), and (2) isolate the

contribution of environmental factors to stream water temperature across this region.

2. Methods

2.1. The Dynamic land Ecosystem model (DLEM)

The terrestrial processes were simulated by the Dynamic Land Ecosystem Model 2.0 (DLEM 2.0) (Fig. 1a), which couples the major terrestrial water cycle (Liu et al., 2013; Pan et al., 2015) with carbon--nitrogen coupled vegetation dynamics (Tian et al., 2012; Chen et al., 2013) to explicitly estimate plant growth, soil biogeochemistry, the associated water fluxes, and greenhouse gas emissions in terrestrial ecosystems driven by the climate forcing and the anthropogenic disturbances. The model has been successfully applied at relatively coarse resolutions such as 0.5 degrees (global level) or five arc-minutes (regional level) (Tian et al., 2015). In order to extend its range to higher resolutions, sub-grid processes were introduced into the terrestrial simulations by adapting a cohort unit. The land-use cohort divides each grid cell into five types of normalized vegetation coverage, including the fraction of cropland, four primary natural vegetation covers, and six non-vegetation types, including urban impervious surface, glacier, lake, stream, ocean water, and bare-ground. DLEM has been previously improved to represent the riverine transport and thus is well suited for quantifying the lateral or vertical fluxes of water, carbon (Tian et al., 2015) and nitrogen (Yao et al., 2020) from land to the oceans (Fig. 1a).

A scale adaptive water transport scheme, MOSART model (Li et al., 2013) was incorporated into the DLEM aquatic module (Yao et al., 2020). The new scheme separates the water transport process within a grid unit into hillslope routing, subnetwork routing, and main channel routing (Fig. 1b). Hillslope routing is the water routing process that aggregates surface runoff and sends it to subnetworks. Groundwater pool receives water from subsurface runoff (shallow groundwater flow) and contributes to subnetworks with outflow rates derived from a fixed residence time, which is empirically set to 2 days (Liu et al., 2013). The subnetwork routing represents the hydrologic processes involving 1st order streams that receive water from overland flow and groundwater pool and then discharge to the main channel. Both hillslope and subnetwork routings are sub-grid routing processes within a grid cell. The main channel routing represents the routing process of higher-order streams (2nd and higher-order streams in a 4-km resolution grid cell for this study) receiving flow from subnetworks and upstream grid cells and flowing to a downstream grid cell.

The DLEM model uses the kinematic wave method for flow routing in channels (Chow, 1964), which requires several hydrography variables (e.g., flow direction, channel length, and channel slope) and geomorphological parameters (e.g., channel width and channel depth). All this information was derived from the hydro1K and NHDplus hydrography datasets (Li et al., 2015a; Yao et al., 2021).

In the water temperature module of DLEM, we simulated the thermal energy dynamics of 1st order (subnetworks in the water transport scheme) and higher-order streams (main channel flow in the water transport scheme) separately. Thus, we need to estimate the water surface area of both types of streams. We obtained the surface area data from remote sensing products for the higher-order streams, and quantified the water surface area (A_s) of 1st order streams (at which scale remotely-sensed products are not available or reliable) through an empirical relationship proposed by Allen et al., 2018:

$$A_{s} = \begin{cases} A_{RS,water}, & remotely - sensed \ d \ ata \\ W \times L, & 1^{st} \ order \ streams \end{cases} \tag{1}$$

$$W = Q^{\frac{3}{5r+3}} \times (0.5A^{0.42})^{\frac{r-1}{r+0.6}} \times \left(8.1(9.8S)^{0.5}k^{-\frac{1}{6}}14^{-\frac{5}{3}}\left(1 - \frac{1}{r+1}\right)\right)^{-\frac{3}{5r+3}}$$
(2)

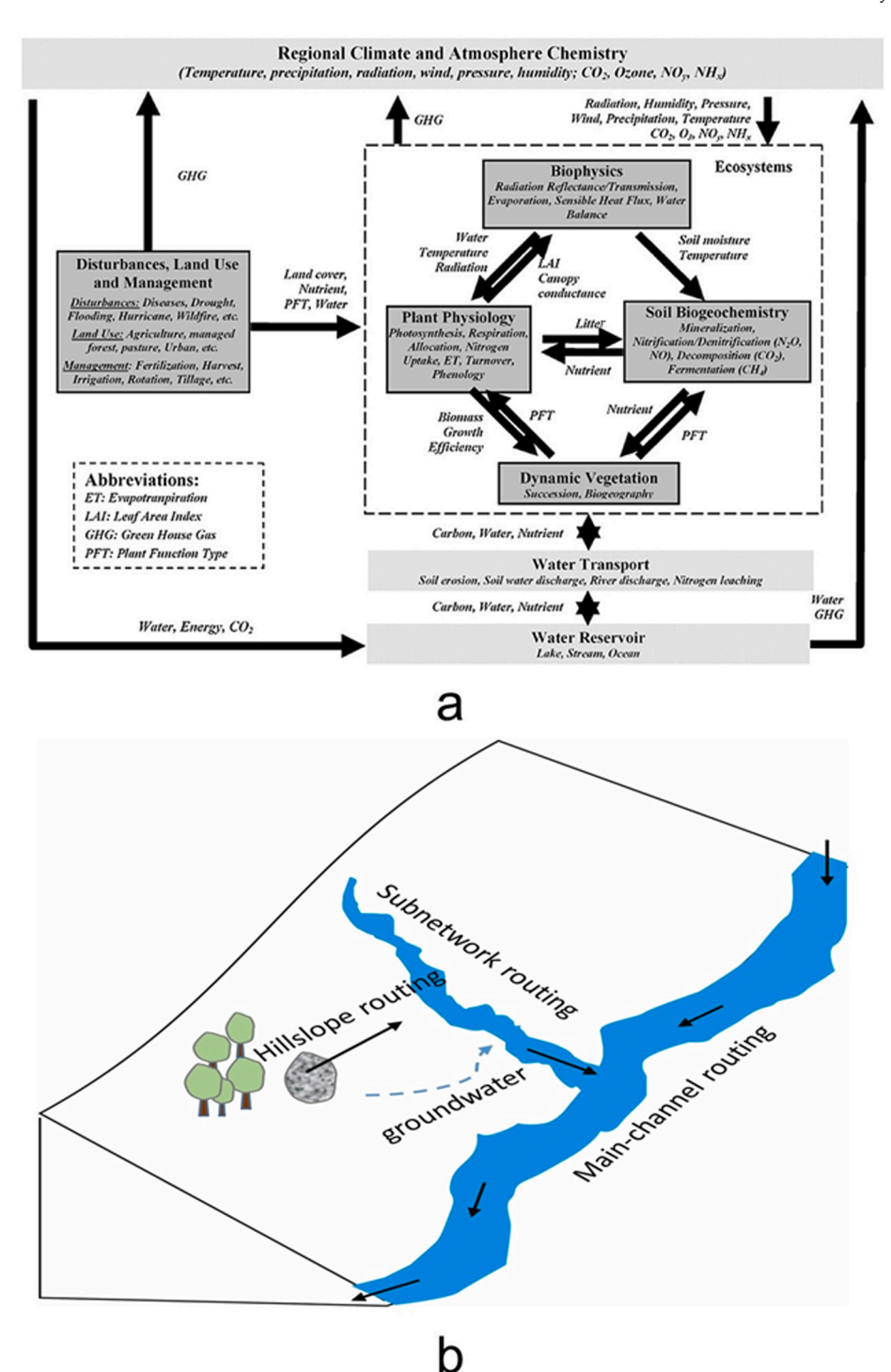


Fig. 1. The general framework of the DLEM Terrestrial/Aquatic Interface Model. (a). The concept model of DLEM. (b). The concept model of MOSART.

where $A_{RS,water}$ denotes the surface area obtained from remote sensing data (m²); W and L represent the channel width and river length of the rivers in the given pixel (m), respectively; A is the drainage area (here we define it as the area of one grid cell) (ha), S is bed slope, Q is water discharge (m³·s⁻¹); r represents the shape parameter (=1.5 following Allen et al., 2018), and k is a bed roughness length scale:

$$k = (8.1g^{0.5}n)^6 (3)$$

in which n is the Manning's roughness coefficient (assumed to be 0.04 s•m $^{-1/3}$), and g is the gravitational acceleration (m•s $^{-2}$).

2.2. Soil temperature module in DLEM

The thermal energy exchange and moisture movement between the soil layers in DLEM were borrowed from the Community Land Model (Bonan et al., 2013). The soil column in DLEM was divided into 10 layers, and the thickness of each layer was defined as 0.05~m, 0.05~m, 0.1~m, 0.2~m, 0.2~m, 0.3~m, 0.3~m, 0.5~m, 0.8~m, and 1.0~m respectively. We did not explicitly quantify the temperature of the vegetation canopy and the heat fluxes between the canopy and the soil surface. Thus, we quantify the surface soil temperature by using a semi-empirical method as the upper boundary condition of the soil layers, which considers the

effect of Leaf Area Index (*LAI*) and litter on soil temperature (Kang et al., 2000):

where ρ_w represents the water density (kg m⁻³), Q_{hil} and Q_g represent the surface runoff from hillslope and subsurface flow (shallow groundwater)

$$\begin{cases}
T_{j} - T_{j-1} = \left[A - T_{j-1}\right] exp\left[-z\left(\frac{\pi}{k_{s}*86400}\right)^{0.5}\right] exp\left[-k_{t} \times (LAI + Litter)\right], when \ A > T_{j-1} \\
T_{j} - T_{j-1} = \left[A - T_{j-1}\right] exp\left[-z\left(\frac{\pi}{k_{s}*86400}\right)^{0.5}\right] exp\left[-k_{t} \times (LAI)\right], when \ A < T_{j-1}
\end{cases}$$
(4)

where A is the 11-day mean daily air temperature (°C), T_j and T_{j-1} are the soil surface temperatures (°C) of the current and the previous days, respectively, k_s is thermal diffusivity (which is set at 0.004 cm²s⁻¹), z is the thickness of the top soil layer (cm), LAI is leaf area index, Litter is the LAI equivalent of ground litter, and k_t is a calibration parameter (dimensionless).

2.3. Water temperature module

We developed a riverine water temperature model within the scale adaptive water transport module and fully coupled it with the soil water temperature model of DLEM (Fig. 2).

The energy balance within a stream segment is given by:

$$\frac{\Delta T}{\Delta t} = \frac{H_a + \left(1 - C_{ef}\right)A_s \times \left(H_s + H_l + H_e + H_c + H_h\right)}{C_w \times M} \tag{5}$$

where C_w represents the specific heat of water (=4186 J/kg °C), M is the total mass of water stored in the channel (kg), and it is calculated as (density)*(volume). Volume is calculated from daily average discharge at the reach, i.e. $(Q_{in} + Q_{out})/2*86400$, where Q_{in} and Q_{out} are average daily inflow to and outflow from the reach, respectively, in cms. C_{ef} is the ratio of water surface area shaded by plant canopies), H_a (W) is the sum of lateral heat fluxes, including thermal inputs from upstream grid cells, local subnetworks, and downstream thermal energy loss. Note that T is in 0 C, and t is in s. In this model, we simulated the lateral heat transport within subnetworks as $(H_a = H_{a.sub})$:

$$H_{a,sub} = \rho_w C_w \times \left(Q_{hil} \left(T_{w,hil} - T_{w,sub} \right) + Q_g \left(T_{w,g} - T_{w,sub} \right) \right) \tag{6}$$

 $(m^3 \cdot s^{-1})$, respectively. $T_{w,hil}$, $T_{w,g}$ and $T_{w,sub}$ represent the water temperature of hillslope flow, groundwater, and subnetworks, respectively. We assume that the water temperature of the hillslope flow is equal to the surface soil temperature. $T_{w,g}$ is defined as the average soil temperature from the surface to a given depth $(D_{w,g})$.

Note that, as a simplification, all the water and heat fluxes from the hillslopes and groundwater pool contribute directly to the first-order streams in the model, i.e., higher-order streams do not receive water or heat flux from hillslopes. This has a minimal effect on results because the total drainage area of hillslopes directly contributing to higher-order streams is a small fraction of the total watershed area (Figure S1).

The lateral heat flux to the main channel($H_a = H_{a.main}$) is given by:

$$H_{a,main} =
ho_{_{W}} C_{_{W}} imes \left(\sum_{i}^{Nup} Q_{up,i} (T_{w,up,i} - T_{w,main}) + Q_{sub} (T_{w,sub} - T_{w,main}) \right)$$
 (7)

where $Q_{up,i}$ is the inflow from up-stream grid cells, $T_{w,main}$ and $T_{w,up,i}$ are the water temperature of upstream inflow and main channel flow, respectively. Nup is the number of upstream grid cells.

 H_s in Eq. (5) is the net shortwave radiation (Wm⁻²) which is set as 97% of the incoming shortwave radiation (H_{s-in}) (Wu et al., 2012), H_l is the net long-wave radiation which is calculated as the difference between incoming longwave radiation (H_{lw-in}) of atmosphere and longwave energy emitted from a water body (H_{lw}) (Thornton and Running, 1999). H_{s-in} and H_{lw-in} were obtained from climate data. H_{lw} is given as:

$$H_{lw} = 0.97 \times \sigma \times (T_w + 273.15)^4 \tag{8}$$

where σ is the Stefan-Boltzmann constant (5.67 \times 10⁻⁸W m⁻²K⁻⁴). H_c represents the riverbed-water specific conductive heat exchange flux (Wm⁻²), set to 5% of the net solar radiative flux (Wu et al., 2012). H_c is

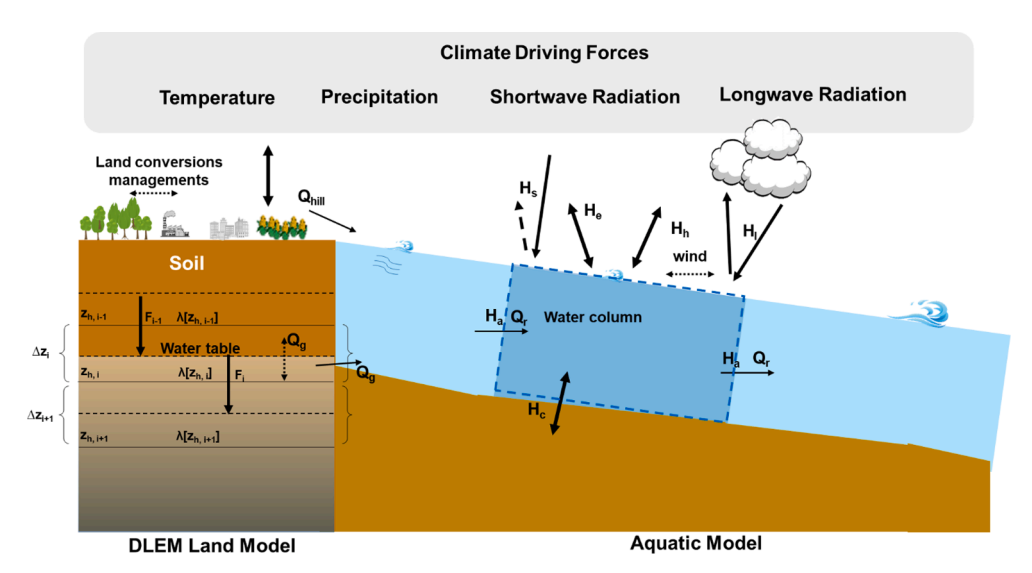


Fig. 2. The framework of DLEM coupled with the water temperature model. Note: F represents heat fluxes, and λ is thermal conductivity.

the specific latent flux (Wm⁻²) estimated as

$$H_e = -\rho_{yy} \times E \times \lambda_e / (86.40 \times 10^6) \tag{9}$$

Here, E represents the evaporation rate of water (mm d⁻¹), λ_e denotes the latent heat flux through vaporization (J kg⁻¹). The evaporation rate is estimated as

$$E = K_l \times (e_{sat} - e) \tag{10}$$

with e_{sat} denoting the saturation vapor pressure (hPa), and e representing the actual vapor pressure (hPa). We quantify K_l from

$$K_l = 0.211 + 0.103 \times V_{wind} \times F_{wind}$$
 (11)

where V_{wind} is the wind speed at 3-meters above the ground/water surface (m·s⁻¹), F_{wind} is a dimensionless factor, which is set at 0.8 (Haag and Luce, 2008). λ_{σ} is given as

$$\lambda_e = 2499.64 - 2.51 \times T_w \tag{12}$$

 H_h is the sensible heat fluxes (Wm⁻²), and can be calculated as (Haag and Luce, 2008)

$$H_h = -\gamma_1 \times \frac{P}{1013} \times K_l \times \lambda_e \times \frac{T_w - T_{air}}{86.40 \times 10^6} \times \rho_w$$
 (13)

where γ_1 represents the psychrometric constant at the standard air pressure, which is set at 0.655 (hPa/°C), *P*denotes the actual air pressure (hPa).

3. Model inputs and simulation experiments

3.1. Study area and model driving forces

The model described above was applied to the Chesapeake Bay Watershed and Delaware River Basin (Fig. 3), both of which are located within the Mid-Atlantic region of the northeast U.S. This is the most urbanized region of the country and sustains more than 25.5 million people. The region covers more than 166,103 square kilometers of land surface and has experienced substantial land conversion due to reforestation over the past century (Hassett et al., 2005).

In this study, we developed a 4-km resolution dataset of this region as model input to run the DLEM model with climate, land conversion, and land management driving forces from 1900 to 2015. A potential vegetation map was reconstructed for the mid-Atlantic region by combining land-use data obtained from the National Land Cover Database (NLCD, Jin et al., 2013) (https://www.mrlc.gov/), the North American Land Change Monitoring System (www.cec.org/naatlas), and the Global C4 vegetation map (Still et al., 2003). We used the county-level inventory data of cropland area and urban area to prescribe the land-use change of natural vegetation (Waisanen and Bliss, 2002). A flowchart describing the generation of the historical land use/land cover is shown in Supplementary Fig. 2. As shown in Fig. 4, cropland area decreased by 57.3% (Fig. 4d) during the past 100 years. This is primarily due to the 9.1% increase in forest area and the 507.5% increase in urban areas. Most of the urban expansion occurred surrounding the megacities, including Washington DC, Baltimore, and Philadelphia (Fig. 4c).

We obtained historical climate variables from the Parameterelevation Relationships on Independent Slopes Model (PRISM) climate

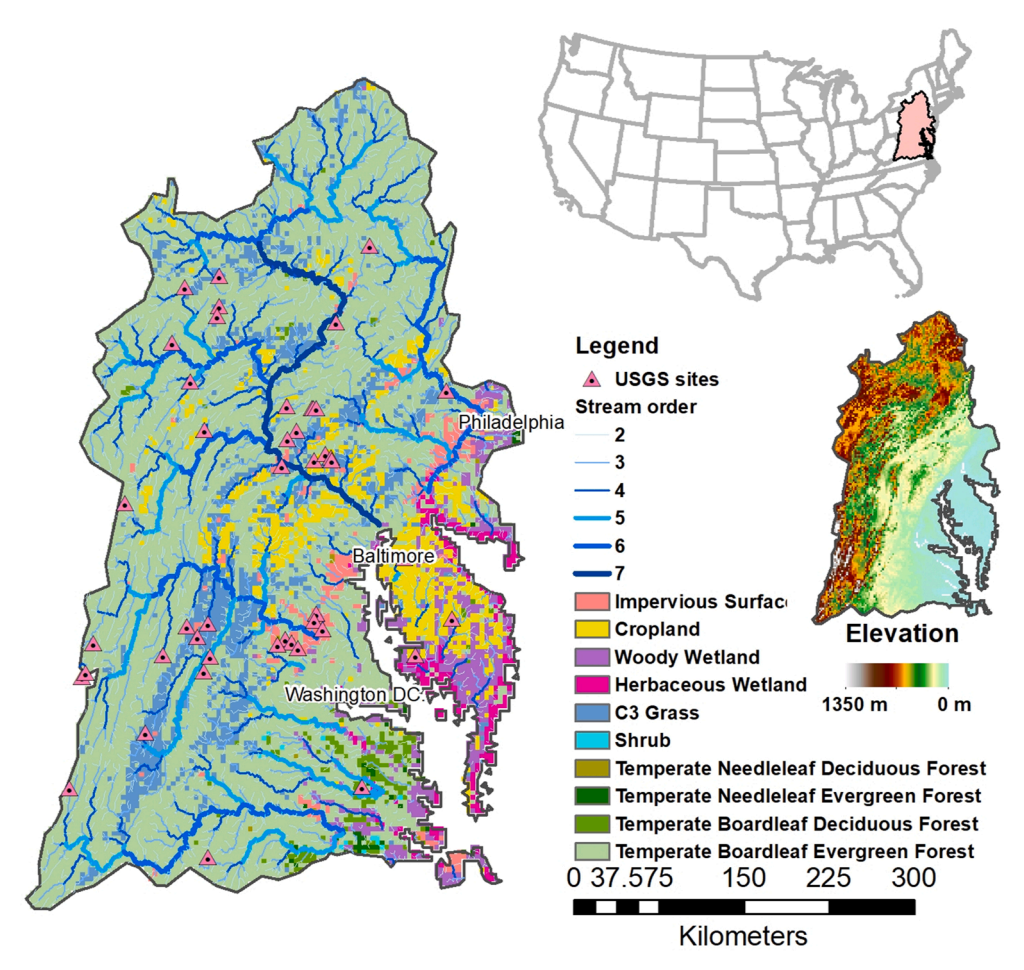


Fig. 3. The major plant function types, land use/land cover and topographic surface in the Mid-Atlantic region.

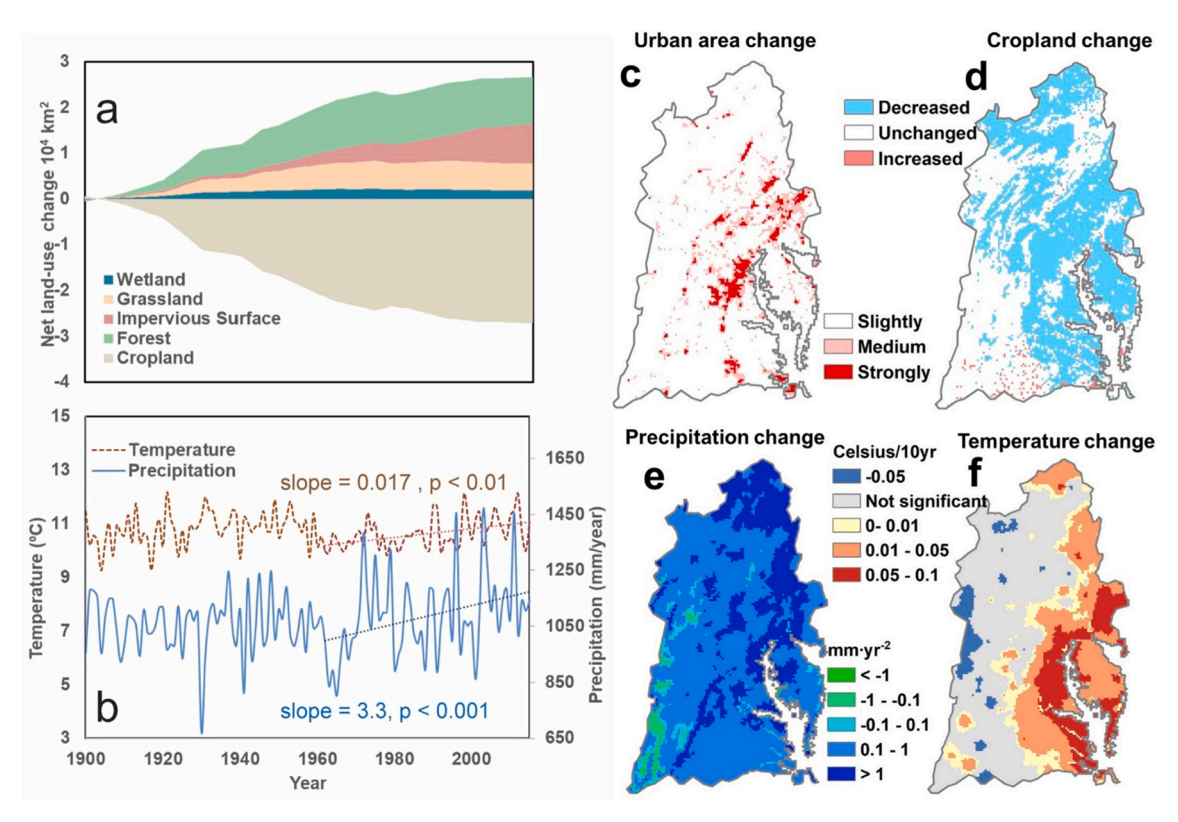


Fig. 4. The spatio-temporal pattern of land conversion and long-term climate change over the Mid-Atlantic region from 1900 to 2015. (a) Temporal pattern of net land-use change from 1900 to 2015, (b) temporal pattern of annual mean precipitation and air temperature from 1900 to 2015, (c) changes in impervious surface, (d) changes in cropland (Note: slightly means up to 10%, medium means up to 30% and strongly means up to 50%), (e) changes in annual total precipitation, and (f) changes in annual mean air temperature.

dataset (available at: http://www.prism.oregonstate.edu/), including daily minimum, mean and maximum temperature, as well as precipitation at 4-km spatial resolution. The mean annual precipitation was $1080.0\pm131.7~\text{mm yr}^{-1}$, and the annual mean temperature was $11.6\pm0.2~^{\circ}\text{C}$ during 1900-2015, respectively. Both precipitation and air temperature show significant increasing trends (p < 0.05, in Mannkendall test) from 1960 to 2015 with the rates of 3.3 $\text{mm} \cdot \text{yr}^{-1}$ and $0.017~^{\circ}\text{C} \cdot \text{decade}^{-1}$, respectively.

The DLEM nitrogen inputs include atmospheric nitrogen deposition, nitrogen fertilizer use, and manure nitrogen production. We combined global nitrogen deposition and Chesapeake Bay Program's data to reconstruct a long-term product (Pan et al., 2021). Crop-specific nitrogen fertilizer use from 1961 to 2008 was obtained from the National Agricultural Statistics Service (https://quickstats.nass.usda.gov/). Manure nitrogen production data was derived from the USDA county-level livestock population data (Yang et al., 2016).

3.2. Simulation experiments

Before running the simulations for the period 1900–2015 at a daily time step, we first set up an equilibrium run for all the grid units. The simulation was forced by the land use data of the year 1900, and the 30-year mean (1900–1929) climate data to represent the pre-industrial environmental conditions. Other driving forces, including atmospheric CO₂ concentration, land use change, and nitrogen inputs, were kept at the pre-industrial levels (1900), to exclude human disturbance. The equilibrium run was terminated when carbon, nitrogen, and water pools reached a steady state (Thornton and Rosenbloom, 2005). After the equilibrium run was completed, we conducted a 30-year spin-up run with randomly selected climate variables from 1900 to 1929. The spin-up run functions as a buffer to smooth the carbon and nitrogen fluxes between the equilibrium run and the year-to-year transient run (Tian et al., 2012). Finally, we conducted a transient run for which all the driving forces change over time from year 1900 to 2015.

We defined three free parameters, including the ones associated with the water surface area (C_{ef} in Eq. (5)) and groundwater inputs (k_t in Eq.

Table 1

The experimental design for attributing changes in water temperature to natural and anthropogenic factors including precipitation, temperature, climate, atmospheric carbon dioxide (CO₂), land-use and nitrogen inputs (including N deposition, N fertilizer, and N manure).

Simulations	Precipitation	Temperature	Climate	CO_2	Land-use	N-inputs
S1	1900-2015	1900-2015	1900-2015	1900-2015	1900-2015	1900-2015
S2	1900-2015	1900-2015	1900-2015	1900-2015	1900-2015	1900
S3	1900-2015	1900-2015	1900-2015	1900-2015	1900	1900-2015
S4	1900-2015	1900-2015	1900-2015	1900	1900-2015	1900-2015
S5	1900-2015	1900-2015	1900	1900-2015	1900-2015	1900-2015
S6	1900-2015	1900	1900-2015	1900-2015	1900-2015	1900-2015
S7	1900	1900-2015	1900-2015	1900-2015	1900-2015	1900-2015

^{*} Climate means the joint effect of precipitation, temperature, relative humidity, shortwave radiation and longwave radiation varying over time.

(4) and $D_{w,g}$ for ground water temperature in equation (6)). We first calibrated k_t (set as 0.5) and $D_{w,g}$ (set as 0.5 m) to match the simulated water temperature of headwater streams to observed water temperature. We then calibrated C_{ef} (ranges from 0.7 - 0.9) of different stream orders to match with the associated observations (Supplementary Table 1).

The simulation with all the driving forces changing over time is recognized as the reference simulation (S 1 in Table 1). We conducted a factorial analysis to assess the contribution of environmental factors to the changes in water temperature. We set up five simulations with each of the environmental factors held constant at year 1900 level (S 2–7 in Table 1), and the contribution of each environmental factor was calculated by comparing the simulated water temperature of each run with the reference simulation. Here, climate effect refers to the joint effect of precipitation, temperature, relative humidity, shortwave radiation, and longwave radiation varying over time. We also examined the effects induced by precipitation and air temperature alone by comparing S 6 and 7 to S 1. For consistency and ease of comparison, all simulations used identical model parameter values, i.e., those calibrated for S 1.

4. Results

4.1. Model performance

To assess the performance of the stream water temperature model, we compared our model simulation results against the daily water temperature measurements at various sites collected by the United States Geological Survey (USGS) (U.S. Geological Survey, 2001). The sites are well distributed in the sub-basins across the region (Fig. 3,

Table 2Daily performance of the physically-based model at selected USGS sites.

USGS site No.		Start year End year 1st order streams		NSE	RMSD (⁰ C)	
01493112	2012	2015	0.90	0.36	4.0	
01537524	2001	2002	0.93	0.80	2.1	
01549100	1973	1977	0.86	0.77	2.8	
01568700	1974	1976	0.77	0.60	3.6	
01575730	1978	1979	0.81	0.76	2.9	
01548303	2012	2015	0.88	0.74	2.8	
01645704	2007	2014	0.95	0.82	2.9	
01645762	2007	2017	0.95	0.82	2.9	
01650800	2012	2013	0.88	0.58	5.1	
01651800	2012	2013	0.87	0.80	1.6	
01654500	2013	2015	0.94	0.84	3.0	
01656903	2007	2015	0.82	0.67	3.9	
02011490	1984	1995	0.89	0.70	3.5	
163626650	2007	2009	0.87	0.79	2.6	
165389205	2011	2014	0.95	0.96	2.9	
	Higher-o	Higher-order streams				
01428750	1989	2004	0.82	0.77	3.2	
01460300	1998	1999	0.90	0.77	3.9	
01463500	1980	2015	0.91	0.90	2.0	
01490120	2006	2009	0.85	0.76	4.4	
01516500	1958	1959	0.88	0.81	4.9	
01547700	1956	1966	0.79	0.48	5.3	
01549300	1973	1977	0.86	0.81	2.7	
01559795	1993	2000	0.87	0.75	2.4	
01564997	1994	1995	0.85	0.70	2.5	
01568750	1974	1976	0.77	0.69	3.3	
01571820	1996	2007	0.76	0.43	4.2	
01573695	2012	2015	0.91	0.83	3.4	
01575741	1978	1979	0.82	0.73	4.3	
01575746	1978	1979	0.78	0.70	4.1	
01610400	2002	2003	0.86	0.69	3.5	
01613900	2007	2008	0.64	0.33	5.6	
01614830	2006	2009	0.91	0.54	3.7	
01621050	2002	2004	0.88	0.48	4.6	
01630700	2006	2009	0.92	0.81	2.9	
01649190	2007	2014	0.88	0.77	3.5	
01673638	2007	2009	0.88	0.68	3.2	
02037500	1950	1956	0.78	0.81	5.1	

Table 2). We calculated Root-Mean-Square Deviation (*RMSD*), Nash-Sutcliffe model efficiency coefficient (*NSE*) (Nash and Sutcliffe, 1970), and Coefficient of Determination (R^2) to assess the performance of the DLEM water temperature model in predicting the daily average water temperature (Table 2, Supplementary Fig. 3). Overall, the modeled water temperatures agree well with the observations. The average R^2 , *NSE*, and *RMSD* values are 0.87, 0.7 and 3.4 °C, respectively (Table 2).

4.2. Spatial and temporal patterns of water temperature

To assess the spatial variation of stream water temperature, we looked at the annual mean water temperatures averaged for the 2006–2015 period. Annual average water temperatures generally vary with latitude, with most of the streams in the south having higher annual mean water temperatures (16 °C - 20 °C) than those in the north (8 °C - 14 °C) (Fig. 5). Topography also plays a role in shaping the spatial pattern of water temperature. As can be seen in Fig. 5, the streams in the Appalachian mountain region have consistently lower temperatures (4 °C–12 °C) than the streams in the coastal plain (12 °C–20 °C), both for 1st order streams and higher-order streams. (Fig. 5).

We analyzed the spatial and temporal pattern of water temperature within the higher-order streams (higher than 1st stream order, Fig. 5a) and 1st order streams (Fig. 5b) separately across the study region. In general, the annual mean water temperatures in the 1st order streams are slightly cooler than the annual mean water temperatures of the higher-order streams. About 68% of the higher-order streams had annual mean water temperature above 12 $^{\circ}\text{C}$. On the contrary, around 57% of the first-order streams had annual mean water temperature below 12 $^{\circ}\text{C}$.

In the megacities (Fig. 3, Fig. 4c), such as Washington DC, Baltimore, and Philadelphia, the annual mean water temperature reached $18\,^{\circ}\text{C}-20\,^{\circ}\text{C}$ in 1st order streams (Fig. 5b), but stream water temperature dropped quickly to $12\,^{\circ}\text{C}-14\,^{\circ}\text{C}$ at higher-order streams (Fig. 5a). In the southeastern part of the study region, the annual mean water temperature of 1st order streams is mostly around $12\,^{\circ}\text{C}-14\,^{\circ}\text{C}$, with the water temperature of the higher-order streams reaching $16\,^{\circ}\text{C}-20\,^{\circ}\text{C}$.

4.3. Long-term changes in stream water temperature

Mean annual water temperature of 1st and higher-order streams were calculated by taking arithmetic averages of each stream segment. Note that each cell contains a 1st order stream and a higher-order stream. The mean annual water temperature in higher-order streams increased significantly (p < 0.05 in Mann-Kendall test) from 1900 to 2015, at a rate of 0.047 °C-decade⁻¹. The warming rate was much higher in recent years (1970–2015) at 0.28 °C-decade⁻¹ (Fig. 6c). The water temperature in 1st order streams also increased significantly (p < 0.05 in Mann-kendall test) during 1900–2015 with a rate of 0.065 °C-decade⁻¹; and the rate reached 0.32 °C-decade⁻¹ from 1970 to 2015 (Fig. 6c). We conducted Student's t-test to compare the average stream temperature of 1st-order and higher-order streams for the period 1900–2015, and found a significant difference (p < 0.01) (Fig. 6c).

We also estimated flow-weighted average water temperature of 1st order and higher-order streams (Supplementary Fig. 4). We found that the increasing trend of water temperature within 1st order streams using the flow-weighted average method (0.31 $^{\circ}\text{C-decade}^{-1}$) is comparable to that of the arithmetic average method (0.32 $^{\circ}\text{C-decade}^{-1}$). However, the increasing trend in temperature in higher-order streams based on the flow-weighted average (0.22 $^{\circ}\text{C-decade}^{-1}$) is much lower than the one based on the arithmetic average (0.28 $^{\circ}\text{C-decade}^{-1}$). For the remainder of the paper, average temperature refers to the arithmetic average.

To check whether these increases are statistically significant, we applied the Mann-Kendall trend test and Theil Sen linear regression to the 116 years of water temperature data at each grid cell (Fig. 6a, b). About 52% of all the stream segments showed warming trend from 1900 to 2015 (p < 0.05) regardless of whether they were first or higher-order

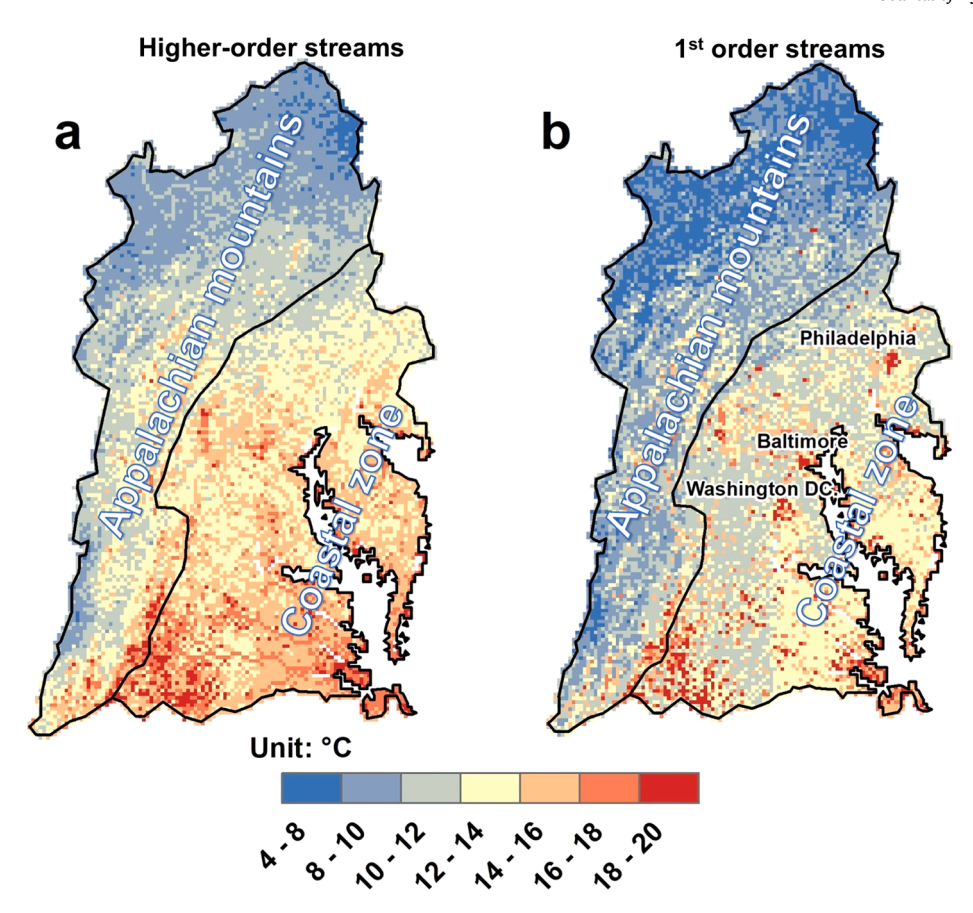


Fig. 5. Spatial pattern of annual average water temperature averaged for the period 2006-2015 for (a) higher-order streams (b) and 1st order streams.

streams (Fig. 6d). The increasing trend of water temperatures in 5th or 6th order streams (Figs. 3, 6a) is not statistically significant (p > 0.05), and the associated trend is less than 0.02 °C•decade⁻¹ from 1900 to 2015. In the inland portions of the study region, stream water temperatures remained relatively stable, with most of the grid cells having statistically insignificant trends (p > 0.05) over the past 116 years (Fig. 6c). However, many 1st order streams showed a century-long increasing trend. Only a few points had a statistically significant (p < 0.05 in Mann-kendall test) decreasing trend of water temperature in both higher-order streams and 1st order streams. The stream water temperature of the northern regions had very small increasing or decreasing trends (mostly p > 0.05), with the rate ranging from -0.001 °C•decade⁻¹ to 0.02C•decade⁻¹. Surprisingly, many of the streams in the southern portion of the study region where the annual average stream temperature is highest (Fig. 6) have a slightly decreasing water temperature, around -0.05 °C•decade⁻¹.

4.4. Attributing the contribution of environmental factors to changes in stream water temperature

The factorial analysis showed that climate factors, i.e., temperature and precipitation, explain about 80% of the changes in stream water temperatures across the mid-Atlantic from 1900 to 2015 (Figs. 7 and 8). In the 1970s, the climate impact on water temperature in higher-order streams and 1st order streams diminished to 30% and 4.4%, respectively (Figs. 7 and 8), primarily due to the similarity of the climate between the 1900s and 1970s. The decadal mean air temperature of the 1900s (10.44 °C) was very close to that of the 1970s (10.53 °C) (Fig. 4). Land-use conversion accounts for 37% and 61% of the changes in water temperature in higher-order streams and 1st order streams, respectively, during the 1970s (Figs. 7 and 8). Nitrogen inputs and increases in atmospheric CO₂ contribute more than 30% of the increase in water

temperature in higher-order streams and 1st order streams in the 1970s. After the 1970s, the contribution of land-use, CO_2 , and N inputs to the changes in water temperature of higher-order streams dropped to $\sim 10\%$, but they still account for $\sim 20\%$ of the changes in 1st order stream water temperature (Fig. 7).

4.5. Sensitivity of stream water temperature in response to the groundwater input

Our model assumes that the temperature of the seepage from groundwater is equal to the mean soil temperature of a defined depth $(D_{w,g} = 0.5 \text{ m})$. To examine the sensitivity of groundwater input parameter on modeled stream water temperature, we run the model $D_{w,g}$ given as 0.1, 0.5, 1 and 2 m, respectively. We then plotted the simulated daily water temperature at two USGS sites of the Delaware River: #01428750 (3rd order) and #01460300 (5th order) (Fig. 9) from 2000 to 2001. This sensitivity analysis suggests that water temperature continuously drops with increased $D_{w,g}$, and a noticeable time lag was detected at both sites when $D_{w,g}$ changed from 0.1 m to 2 m, especially for the Delaware River sites located at higher-order streams. We compared the model performances for different $D_{w,g}$ values. The performances were similar for $D_{w,g} = 0.1$ m and 0.5 m (R² = 0.77, NSE = 0.71, RMSD = 3.9 for 0.1 m; R² = 0.76, NSE = 0.7, RMSD = 4.0 for 0.5 m). The model performance decreased significantly once $D_{w,g}$ became larger than 0.5 m ($R^2 = 0.7$, NSE = 0.64, RMSD = 4.4 for $D_{w,g} = 1$ m; R^2 = 0.58, NSE = 0.53, RMSD = 5.0 for $D_{w,g} = 2m$).

5. Discussion

5.1. The impact of climate on the stream water temperature

Air temperature is the dominant driver of the increase and variability

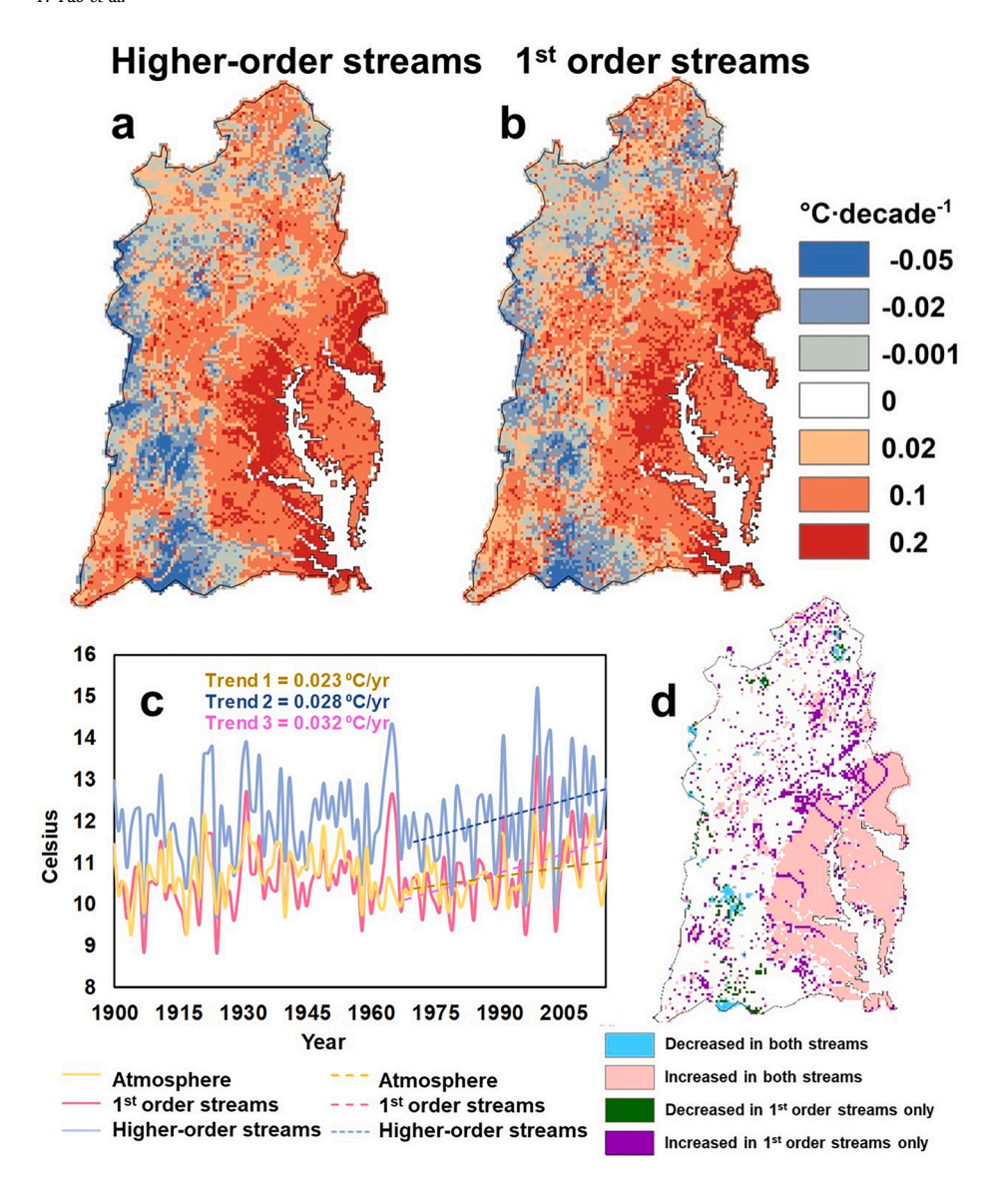


Fig. 6. Changes (1900–2015) in mean annual water temperature within (a) higher-order streams, (b) 1st order streams, and (c) across the Mid-Atlantic region. (d) Significance of long-term changes in water temperature of 1st order streams and higher-order streams (p < 0.05 in Man-Kendal trend test). Note: The trends in (c) are the rates of increase of arithmetic-averaged air temperature (trend 1), water temperatures in higher-order streams (trend 2) and water temperature in 1st order streams (trend 3) from 1960 to 2015

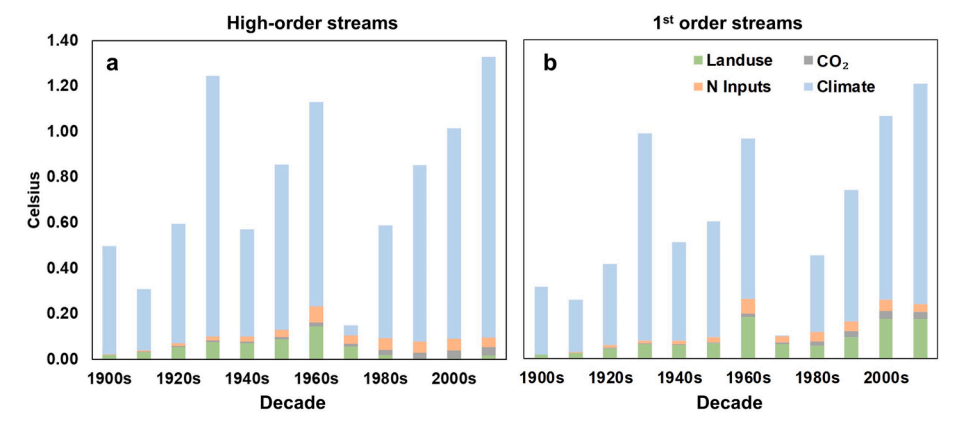


Fig. 7. Contribution of environmental factors to the changes in water temperature in (a) higher-order streams and (b) 1st order streams.

in stream water temperature. The spatial pattern of the warming trend of water temperature (Fig. 6d) follows that of air temperature (Fig. 4f), with both water and air temperatures increasing in coastal regions and decreasing in the mountain regions. Air temperature primarily influences water temperature in two pathways: (1) thermal energy is

exchanged between the air and water interface (Arismendi et al., 2014), and (2) rising air temperature influences land surface temperature and indirectly impacts the temperature of shallow groundwater and the adjacent 1st order streams (Kurylyk et al., 2015; Menberg et al., 2014). Using data from 129 USGS sites, Rice and Jastram (2015) found that

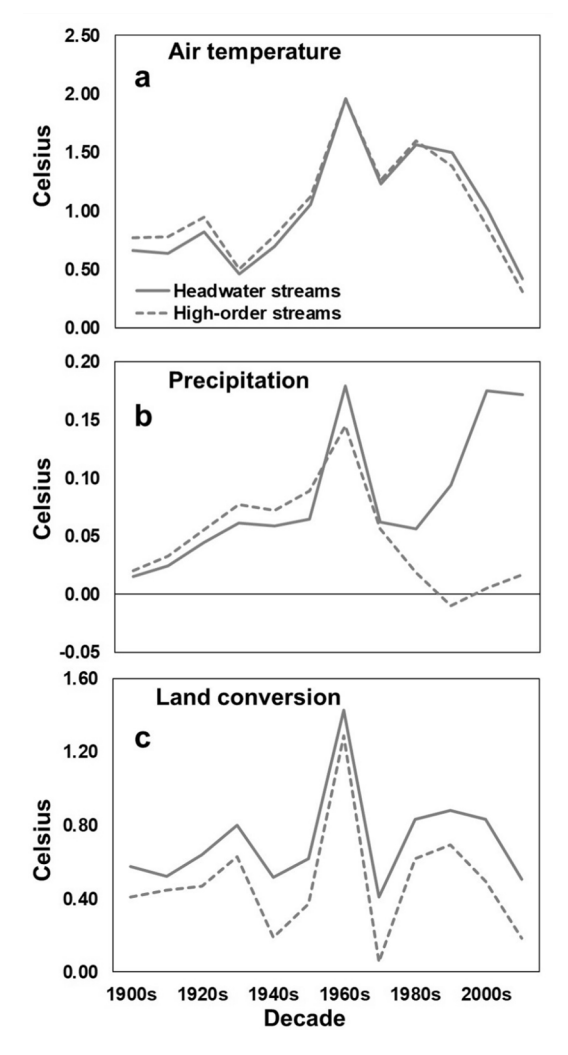


Fig. 8. Changes in water temperature of 1st order streams and higher-order streams across the Mid-Atlantic region in response to (a) air temperature, (b) precipitation, and (c) land-use conversion.

since the 1970s, stream water temperatures and air temperature across the Chesapeake Bay Watershed are increasing at statistically significant (p < 0.05 in Mann-kendall test) rates, at $0.28 \, ^{\circ}\text{C-decade}^{-1}$ and $0.23 \, ^{\circ}\text{C-decade}^{-1}$, respectively. Since most of the observation sites in Rice and Jastram's (2015) study were located in higher-order streams, the magnitude of the increasing trend in their study is consistent with the DLEM estimated rate of increase ($0.28 \, ^{\circ}\text{C-decade}^{-1}$) of water temperature in higher-order streams from 1970 to 2015 across the whole Mid-Atlantic region; however, DLEM-based results suggest a higher rate of increase of water temperature ($0.32 \, ^{\circ}\text{C-decade}^{-1}$) in 1st order

streams.

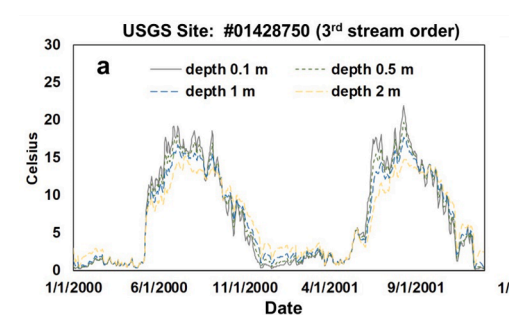
Overall, the contribution of air temperature to the changes in water temperature in higher-order streams is consistent with that of 1st order streams in our factorial analysis (Fig. 8a). Thus, the higher rate of increase of water temperature in 1st order streams must come from other environmental factors. Precipitation is another dominant climate variable that significantly influences stream water temperature. A higher precipitation rate would enlarge the water surface area in the headwater zone, which accelerates the thermal energy exchange between air and water (equation (5)). On the other hand, the increase in precipitation results in cooling of groundwater discharge in summer and warming in winter (Briggs et al., 2018), which substantially buffers the seasonal variations of water temperature in both 1st order and higher-order streams (Burns et al., 2017; Snyder et al., 2015). Additionally, increased precipitation cools the land surface even though evaporative energy release also contributes to the changes in water temperature (Trenberth and Shea, 2005).

Our factorial experiments suggest that the contribution of precipitation to 1st order stream temperature is more significant than that for higher-order streams (Fig. 8b). We only considered the contribution of the absolute value of air temperature and precipitation because of the variations in climate conditions that do not account for the long-term changes. That is because the increased precipitation substantially increased groundwater discharge. The 1st order streams, which have considerable groundwater and surface water exchanges, show less seasonal variation than the main river channels. Thus, 1st order streams are conventionally thought of as a refugia for species, in relation to climate change, due to the cooling effect of groundwater discharge during the summer season (Ficklin et al., 2014; Isaak et al., 2016; Snyder et al., 2015)

A recent study found that the thermal energy of water seepage from shallow groundwater increased significantly with the rising land-surface temperature in the Blue Ridge Mountains of the U.S. (Briggs et al., 2018). The refugia of cold water species would disappear soon due to global warming (Leach and Moore, 2019). Similarly, we found a faster rate of increase of temperature in groundwater-fed 1st order streams across the Mid-Atlantic region (Fig. 6c). Leach and Moore (2019) also reached a similar conclusion at the catchment level using a process-based study.

5.2. Land conversion effects on water temperature

Land-use change shows a tremendous impact on water temperature in higher-order streams and 1st order streams. As predicted by DLEM, water temperature in urban streams reached $18\,^{\circ}\text{C}-20\,^{\circ}\text{C}$ in 2015, which is higher than the water temperature of the sub-urban regions (Fig. 5b). Simulation results suggest that water temperature in 1st order streams is susceptible to urbanization. However, the effect of land-use change on water temperatures quickly dampened while water flows into 2nd or higher-order streams (Fig. 5a) because the contribution of advective heat fluxes on water temperature was significantly enhanced due to the



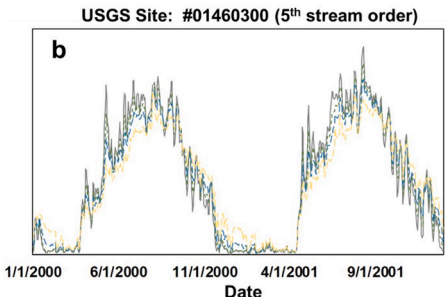


Fig. 9. Simulated water temperature at the outlet of the (a) Delaware River, and (b) Susquehanna river in response to various options for setting the groundwater boundary conditions.

increased water surface area.

The study region experienced a significant re-forestation from cropland and de-forestation due to urbanization during the last century (Fig. 4a), which contributed to the substantial changes in water temperature. That is because we considered the effects of plant LAI on soil surface temperature (equation (5)), which could have cascading effects on the water temperature in 1st order streams and higher-order streams. Forests have higher LAI than that of cropland and urban impervious surface, and this shading effect of forest canopy results in cooler waters in the mountain region (Fig. 5). On the other hand, the changes in vegetation types resulted in different ground litter depth and surface albedo, which are directly linked to the soil evaporative energy release. We found that water temperature in areas dominated by forests or grassland is much lower than in urban areas due to the higher evapotranspiration rates, which has been implicitly represented in DLEM (Fig. 5). Additionally, we found a significant warmer water temperature in 1st order streams adjacent to the megacities (Fig. 6 a, b). These stream temperature surges directly link to the loss of biomass cover and a warmer air temperature (urban heat island) due to rapid urbanization, which is also supported by the catchment scale modeling and field observation studies (LeBlanc et al., 1997; Nelson et al., 2009; Nelson and Palmer, 2007).

5.3. Effect of groundwater on water temperature

Earth system models and hydrological models do not explicitly simulate the lateral transport of groundwater from the soil root zone to the tributary streams. Thus, simplification is needed in the definition of the 1st order stream temperatures or seepage groundwater temperature. Most of the previous modeling studies used empirical models to represent the water temperature of the headwater zone. The empiricallybased headwater temperature estimates were used as boundary conditions to force the water temperature models (Brown, 1969; Van Vliet et al., 2013; Van Vliet et al., 2012; Van Wijk and De Vries, 1963; Wanders et al., 2019; Wu et al., 2012). Thus, the sensitivity of water temperature in response to the boundary condition has not been thoroughly investigated. Especially for the large rivers (4th and higher), climatic and hydraulics variables including surface area, air temperature, and radiation were conventionally considered as the dominant drivers (Li et al., 2015b; Wu et al., 2012). Therefore, proper representation of the temperature of the seepage from groundwater is of great importance during the coupling of the land model with riverine transport. Li et al. (2015a) suggested that the boundary condition of the groundwater seepage temperature is from the water table to the bottom of the root zone (5 m depth in the Community Land Model (Oleson et al., 2010)), which is much deeper than that in this study. Coupling of surface and ground water processes will be needed in the future for improved water temperature estimates in streams, as the depth of the water table may be very different in different topographies and climates.

5.4. Comparison to other models

The DLEM water temperature module has a comparable performance to other representative models conducted at different scales (Ficklin et al., 2012; Van Vliet et al., 2012; Wu et al., 2012; Yearsley, 2012). The average NSE of the previous studies varies from 0.50 to 0.70, which is slightly lower than the values in this study. The ranges of R² and RMSD in previous studies are about 0.8–0.9 and 2.0–4.0, respectively, which are in agreement with our results. However, improving the prediction of stream water temperature was not the primary goal of this study. This is the first study, to our knowledge, that fully coupled a terrestrial ecosystem model with a physically-based water temperature model.

Empirically-based models, which commonly use air temperature as the sole variable to predict the water temperature, can achieve a better accuracy over process-based models because their simple structures allow adequate parameterization (Brown, 1969; Chen and Fang, 2015b; Mohseni et al., 1998; Segura et al., 2014; Wehrly et al., 2009). However, there is a growing debate on if air temperature could be used as the sole indicator of water temperature (Arismendi et al., 2014); the reliability of empirical equations would be substantially hampered by the changes in hydrological conditions or land use/cover (Arismendi et al., 2014). Our study showed that the rate of increase of water temperature in 1st order streams is higher than that of air temperature (Fig. 6 c), which cannot be captured by empirical models. This, and other findings imply that empirical equations may not be reliable for long-term predictions due to the lack of mechanistic representation, which is also supported by a catchment level study within the Columbia river basin (Leach and Moore, 2019).

5.5. Uncertainties and future work

Although this model is process-based, we still used several semiempirical equations to represent the physical processes. For instance, we conducted a semi-empirical based method to estimate the water surface area (Allen et al., 2018). Additionally, the model parameters may have significant uncertainties, which have not been investigated in this study.

Human activities, such as water extraction, or point source discharges, were not considered in the model. Water extraction from groundwater and stream water are ubiquitous agricultural activities, significantly affecting soil evaporation, groundwater outflow, and even soil properties (Keery et al., 2007). In this study, we investigated the effect of changes in CO2 and nitrogen inputs on stream water temperature (primarily through the effect of plant growth). Although these human-induced factors individually only provide minor contributions to the increase of water temperature and the impact of the CO₂ fertilization effect is still being debated, the combination of those effects is considerable. Moreover, a noticeable increasing trend of these human-induced effects was found in 1st order streams, which local studies also support. (Terrer et al., 2016). Furthermore, hot water releases from industry, considered as thermal pollutants, can strongly affect the health of aquatic ecosystems (Webb et al., 2008). Unfortunately, it is not yet possible to incorporate this effect into the model due to the lack of century-long data. Although we do not have large lakes and reservoirs in our study area, future studies in different regions may have to consider the impact of dams and lakes. The cooling effect of dams has been well documented in observations and modeling studies (Chen and Fang, 2015a; King et al., 1998). However, the warming effect of dams is a debated topic too (He et al., 2020; Kędra and Wiejaczka, 2018).

6. Conclusions

In this study, we investigated changes in stream water temperature by developing a water temperature module within the DLEM modeling framework. By linking the thermal energy balance of land and aquatic systems together, this framework can address how land processes will likely affect water discharge and water temperature in the future. Here we applied and evaluated this model to the mid-Atlantic region of the U. S., filling a fundamental knowledge gap relating the impacts of climate and human disturbances on the water temperature of 1st and higher-order streams. We found that although climate variability is the dominant factor in regulating stream water temperature, other environmental factors, including land-use conversions, increased atmospheric CO₂, and nitrogen management efforts also play active roles in this problem, especially for 1st order streams. The rate of water temperature increase in 1st order streams is faster than that of higher-order streams, suggesting a hidden risk for local freshwater biodiversity.

Future research will explore how changes in stream water temperatures will likely impact aquatic biogeochemistry in these systems. Since the study region does not have large lakes and reservoirs, the missing component to represent the dam and lake routing and stratification would not influence the reliability of the model. With the improved technology and increased availability of data, remote sensing-based methods are also prompting a new direction for estimating stream water temperature (Martí-Cardona et al., 2019). Better data-model integrations in the future will likely enhance model capability in predicting 1st order stream and higher-order stream water temperature and the associated biogeochemical cycles.

7. Data availability statements

The relevant datasets of this study are archived in the box site of International Center for Climate and Global Change Research at Auburn University (https://auburn.box.com/v/CBWstreamtemp).

CRediT authorship contribution statement

HT: conceptualization and investigation, supervision, Funding acquisition, project administration and resources, write original draft. YY: conceptualization and investigation, formal analysis and methodology, write original draft. LK: supervision, write original draft. SP: supervision. JW: validation. YL: validation. MF: Funding acquisition, project administration and resources, and all coauthors review and edit the manuscript.

Declaration of Competing Interest

The authors declare that they have no known competing financial interests or personal relationships that could have appeared to influence the work reported in this paper.

Acknowledgements

This study is the results of research funded in part by NOAA National Centers for Coastal Ocean Science (award number: NA16NOS4780207), NASA Interdisciplinary Science Program (award numbers: NNX11AD47G; NNX14AF93G) and National Science Foundation (award number: 1903722).

Appendix A. Supplementary data

Supplementary data to this article can be found online at https://doi.org/10.1016/j.jhydrol.2021.126633.

References

- Allen, G.H., Pavelsky, T.M., Barefoot, E.A., Lamb, M.P., Butman, D., Tashie, A., Gleason, C.J., 2018. Similarity of stream width distributions across headwater systems. Nat. Commun. 9, 610.
- Arismendi, I., Safeeq, M., Dunham, J.B., Johnson, S.L., 2014. Can air temperature be used to project influences of climate change on stream temperature? Environ. Res. Lett. 9 (8), 084015. https://doi.org/10.1088/1748-9326/9/8/084015.
- Bonan, G.B., Drewniak, B., Huang, M., Koven, C.D., Levis, S., Li, F., Riley, W.J., Subin, Z. M., Swenson, S.C., Thornton, P.E., 2013. Technical description of version 4.5 of the Community Land Model (CLM). NCAR Tech Note NCARTN-503 STR Natl.
- Briggs, M.A., Lane, J.W., Snyder, C.D., White, E.A., Johnson, Z.C., Nelms, D.L., Hitt, N.P., 2018. Shallow bedrock limits groundwater seepage-based headwater climate refugia. Limpologica 68, 142–156.
- Brown, G.W., 1969. Predicting temperatures of small streams. Water Resour. Res. 5 (1), 68–75.
- Brown, G.W., Krygier, J.T., 1970. Effects of clear-cutting on stream temperature. Water Resour. Res. 6 (4), 1133–1139.
- Buccola, N.L., Turner, D.F., Rounds, S.A., 2016. Water temperature effects from simulated dam operations and structures in the Middle Fork Willamette River, western Oregon. US Geological Survey.
- Burns, E.R., Zhu, Y., Zhan, H., Manga, M., Williams, C.F., Ingebritsen, S.E., Dunham, J.B., 2017. Thermal effect of climate change on groundwater-fed ecosystems. Water Resour. Res. 53 (4), 3341–3351.
- Butman, D., Raymond, P.A., 2011. Significant efflux of carbon dioxide from streams and rivers in the United States. Nat. Geosci. 4 (12), 839–842.
- Chapra, S.C., 2008. Surface water-quality modeling. Waveland press.
- Chen, D., Hu, M., Guo, Y.i., Dahlgren, R.A., 2016. Changes in river water temperature between 1980 and 2012 in Yongan watershed, eastern China: Magnitude, drivers and models. J. Hydrol. 533, 191–199.

- Chen, G., Fang, X., 2015a. Sensitivity analysis of flow and temperature distributions of density currents in a river-reservoir system under upstream releases with different durations. Water 7 (11), 6244–6268.
- Chen, G., Fang, X., 2015b. Accuracy of hourly water temperatures in rivers calculated from air temperatures. Water 7 (12), 1068–1087.
- Chen, G., Tian, H., Huang, C., Prior, S.A., Pan, S., 2013. Integrating a process-based ecosystem model with Landsat imagery to assess impacts of forest disturbance on terrestrial carbon dynamics: case studies in Alabama and Mississippi. J. Geophys. Res. Biogeosciences 118 (3), 1208–1224.
- Chow, V.T., 1964. Handbook of applied hydrology. Section 8, 8-61.
- Claireaux, G., Webber, D.M., Lagardère, J.-P., Kerr, S.R., 2000. Influence of water temperature and oxygenation on the aerobic metabolic scope of Atlantic cod (Gadus morhua). J. Sea Res. 44 (3-4), 257–265.
- Cover, M.R., de la Fuente, J.A., Resh, V.H., 2010. Catastrophic disturbances in headwater streams: the long-term ecological effects of debris flows and debris floods in the Klamath Mountains, northern California. Can. J. Fish. Aquat. Sci. 67 (10), 1596–1610. https://doi.org/10.1139/F10-079.
- Ficklin, D.L., Barnhart, B.L., Knouft, J.H., Stewart, I.T., Maurer, E.P., Letsinger, S.L., Whittaker, G.W., 2014. Climate change and stream temperature projections in the Columbia River basin: habitat implications of spatial variation in hydrologic drivers. Hydrol. Earth Syst. Sci. 18 (12), 4897–4912. https://doi.org/10.5194/hess-18-4897-2014.
- Ficklin, D.L., Luo, Y., Stewart, I.T., Maurer, E.P., 2012. Development and application of a hydroclimatological stream temperature model within the Soil and Water Assessment Tool. Water Resour Res. 48 (1) https://doi.org/10.1029/ 2011WR011256.
- Haag, I., Luce, A., 2008. The integrated water balance and water temperature model LARSIM-WT. Hydrol. Process. Int. J. 22 (7), 1046–1056.
- Harrison, J.A., Maranger, R.J., Alexander, R.B., Giblin, A.E., Jacinthe, P.-A., Mayorga, E., Seitzinger, S.P., Sobota, D.J., Wollheim, W.M., 2009. The regional and global significance of nitrogen removal in lakes and reservoirs. Biogeochemistry 93 (1-2), 143–157.
- Hassett, B., Palmer, M., Bernhardt, E., Smith, S., Carr, J., Hart, D., 2005. Restoring watersheds project by project: trends in Chesapeake Bay tributary restoration. Front. Ecol. Environ. 3 (5), 259–267.
- He, T., Deng, Y., Tuo, Y., Yang, Y., Liang, N., 2020. Impact of the dam construction on the downstream thermal conditions of the Yangtze River. Int. J. Environ. Res. Public. Health 17 (8), 2973. https://doi.org/10.3390/ijerph17082973.
- Isaak, D.J., Luce, C.H., Rieman, B.E., Nagel, D.E., Peterson, E.E., Horan, D.L., Parkes, S., Chandler, G.L., 2010. Effects of climate change and wildfire on stream temperatures and salmonid thermal habitat in a mountain river network. Ecol. Appl. 20 (5), 1350–1371.
- Isaak, D.J., Wenger, S.J., Peterson, E.E., Ver Hoef, J.M., Nagel, D.E., Luce, C.H., Hostetler, S.W., Dunham, J.B., Roper, B.B., Wollrab, S.P., Chandler, G.L., Horan, D. L., Parkes-Payne, S., 2017. The NorWeST summer stream temperature model and scenarios for the western US: a crowd-sourced database and new geospatial tools foster a user community and predict broad climate warming of rivers and streams. Water Resour. Res. 53 (11), 9181–9205.
- Isaak, D.J., Young, M.K., Luce, C.H., Hostetler, S.W., Wenger, S.J., Peterson, E.E., Ver Hoef, J.M., Groce, M.C., Horan, D.L., Nagel, D.E., 2016. Slow climate velocities of mountain streams portend their role as refugia for cold-water biodiversity. Proc. Natl. Acad. Sci. 113 (16), 4374–4379.
- Jin, S., Yang, L., Danielson, P., Homer, C., Fry, J., Xian, G., 2013. A comprehensive change detection method for updating the National Land Cover Database to circa 2011. Remote Sens. Environ. 132, 159–175.
- Kang, S., Kim, S., Oh, S., Lee, D., 2000. Predicting spatial and temporal patterns of soil temperature based on topography, surface cover and air temperature. For. Ecol. Manag. 136 (1-3), 173–184.
- Kędra, M., Wiejaczka, Ł., 2018. Climatic and dam-induced impacts on river water temperature: Assessment and management implications. Sci. Total Environ. 626, 1474–1483
- Keery, J., Binley, A., Crook, N., Smith, J.W.N., 2007. Temporal and spatial variability of groundwater–surface water fluxes: development and application of an analytical method using temperature time series. J. Hydrol. 336 (1-2), 1–16.
- King, J., Cambray, J.A., Impson, N.D., 1998. Linked effects of dam-released floods and water temperature on spawning of the Clanwilliam yellowfish Barbus capensis. Hydrobiologia 384, 245–265.
- Koontz, E.D., Steel, E.A., Olden, J.D., 2018. Stream thermal responses to wildfire in the Pacific Northwest. Freshw. Sci. 37 (4), 731–746. https://doi.org/10.1086/700403.
- Kurylyk, B.L., MacQuarrie, K.T.B., Caissie, D., McKenzie, J.M., 2015. Shallow groundwater thermal sensitivity to climate change and land cover disturbances: derivation of analytical expressions and implications for stream temperature modeling. Hydrol. Earth Syst. Sci. 19 (5), 2469–2489. https://doi.org/10.5194/hess-19-2469-2015.
- Leach, J.A., Moore, R.D., 2019. Empirical stream thermal sensitivities may underestimate stream temperature response to climate warming. Water Resour. Res. 55 (7), 5453–5467. https://doi.org/10.1029/2018WR024236.
- LeBlanc, R.T., Brown, R.D., FitzGibbon, J.E., 1997. Modeling the effects of land use change on the water temperature in unregulated urban streams. J. Environ. Manage. 49 (4), 445–469.
- Li, H., Wigmosta, M.S., Wu, H., Huang, M., Ke, Y., Coleman, A.M., Leung, L.R., 2013. A physically based runoff routing model for land surface and earth system models. J. Hydrometeorol. 14, 808–828. https://doi.org/10.1175/JHM-D-12-015.1.
- Li, H.-Y., Leung, L.R., Getirana, A., Huang, M., Wu, H., Xu, Y., Guo, J., Voisin, N., 2015a. Evaluating global streamflow simulations by a physically based routing model

- coupled with the community land model. J. Hydrometeorol. 16, 948–971. https://doi.org/10.1175/JHM-D-14-0079.1.
- Li, H.-Y., Ruby Leung, L., Tesfa, T., Voisin, N., Hejazi, M., Liu, L.u., Liu, Y., Rice, J., Wu, H., Yang, X., 2015b. Modeling stream temperature in the Anthropocene: an earth system modeling approach: MODELING STREAM TEMPERATURE IN ESM. J. Adv. Model. Earth Syst. 7 (4), 1661–1679. https://doi.org/10.1002/2015MS000471
- Liu, M., Tian, H., Yang, Q., Yang, J., Song, X., Lohrenz, S.E., Cai, W.-J., 2013. Long-term trends in evapotranspiration and runoff over the drainage basins of the Gulf of Mexico during 1901–2008. Water Resour. Res. 49 (4), 1988–2012. https://doi.org/ 10.1002/wrcr.20180.
- Martí-Cardona, B., Prats, J., Niclòs, R., 2019. Enhancing the retrieval of stream surface temperature from Landsat data. Remote Sens. Environ. 224, 182–191. https://doi. org/10.1016/j.rse.2019.02.007.
- McQueen, D.J., Lean, D.R.S., 1987. Influence of water temperature and nitrogen to phosphorus ratios on the dominance of blue-green algae in Lake St. George. Ontario. Can. J. Fish. Aquat. Sci. 44 (3), 598–604.
- Menberg, K., Blum, P., Kurylyk, B.L., Bayer, P., 2014. Observed groundwater temperature response to recent climate change. Hydrol. Earth Syst. Sci. 18, 4453–4466. https://doi.org/10.5194/hess-18-4453-2014.
- Mohseni, O., Stefan, H.G., Erickson, T.R., 1998. A nonlinear regression model for weekly stream temperatures. Water Resour. Res. 34 (10), 2685–2692. https://doi.org/ 10.1029/98WR01877.
- Nash, J.E., Sutcliffe, J.V., 1970. River flow forecasting through conceptual models part I — A discussion of principles. J. Hydrol. 10 (3), 282–290. https://doi.org/10.1016/ 0022-1694(70)90255-6.
- Nelson, K.C., Palmer, M.A., 2007. Stream temperature surges under urbanization and climate change: Data, models, and responses. JAWRA J. Am. Water Resour. Assoc. 43 (2), 440–452
- Nelson, K.C., Palmer, M.A., Pizzuto, J.E., Moglen, G.E., Angermeier, P.L., Hilderbrand, R. H., Dettinger, M., Hayhoe, K., 2009. Forecasting the combined effects of urbanization and climate change on stream ecosystems: from impacts to management options. J. Appl. Ecol. 46, 154–163.
- Nepstad, D.C., Stickler, C.M., Filho, B., Merry, F., 2008. Interactions among Amazon land use, forests and climate: prospects for a near-term forest tipping point. Philos. Trans. R. Soc. B Biol. Sci. 363 (1498), 1737–1746.
- Oleson, K.W., Lawrence, D.M., Gordon, B., Flanner, M.G., Kluzek, E., Peter, J., Levis, S., Swenson, S.C., Thornton, E., Feddema, J., 2010. Technical description of version 4.0 of the Community Land Model (CLM).
- Pan, S., Tian, H., Dangal, S.R., Yang, Q., Yang, J., Lu, C., Tao, B., Ren, W., Ouyang, Z., 2015. Responses of global terrestrial evapotranspiration to climate change and increasing atmospheric CO₂ in the 21st century. Earths Future 3, 15–35.
- Pan, S., Bian, Z., Tian, H., Yao, Y., Najjar, R.G., Friedrichs, M.A., Hofmann, E.E., Xu, R., Zhang, B., 2021. Impacts of Multiple Environmental Changes on Long-term Nitrogen Loading from the Chesapeake Bay Watershed. J. Geophys. Res.: Biogeosci. e2020.IG005826.
- Pastor, J., Solin, J., Bridgham, S.D., Updegraff, K., Harth, C., Weishampel, P., Dewey, B., 2003. Global warming and the export of dissolved organic carbon from boreal peatlands. Oikos 100 (2), 380–386.
- Rice, K.C., Jastram, J.D., 2015. Rising air and stream-water temperatures in Chesapeake
 Bay region, USA, Clim, Change 128 (1-2), 127–138.
- Sander, R., 2015. Compilation of Henry's law constants (version 4.0) for water as solvent. Atmospheric Chem. Phys. 15 (8), 4399–4981. https://doi.org/10.5194/acp-15.4390-2015
- Segura, C., Caldwell, P., Sun, G.e., McNulty, S., Zhang, Y., 2014. A model to predict stream water temperature across the conterminous USA. Hydrol. Process. 29 (9), 2178–2195. https://doi.org/10.1002/hyp.10357.
- Snyder, C.D., Hitt, N.P., Young, J.A., 2015. Accounting for groundwater in stream fish thermal habitat responses to climate change. Ecol. Appl. 25 (5), 1397–1419. https:// doi.org/10.1890/14-1354.1.

- Still, C.J., Berry, J.A., Collatz, G.J., DeFries, R.S., 2003. Global distribution of C3 and C4 vegetation: carbon cycle implications 17, 6-1-6-14.
- Terrer, C., Vicca, S., Hungate, B.A., Phillips, R.P., Prentice, I.C., 2016. Mycorrhizal association as a primary control of the CO₂ fertilization effect. Science 353 (6294), 72–74
- Thornton, P.E., Rosenbloom, N.A., 2005. Ecosystem model spin-up: Estimating steady state conditions in a coupled terrestrial carbon and nitrogen cycle model. Ecol. Model. 189 (1-2), 25–48. https://doi.org/10.1016/j.ecolmodel.2005.04.008.
- Thornton, P.E., Running, S.W., 1999. An improved algorithm for estimating incident daily solar radiation from measurements of temperature, humidity, and precipitation. Agric. For. Meteorol. 93 (4), 211–228.
- Tian, H., Chen, G., Zhang, C., Liu, M., Sun, G.e., Chappelka, A., Ren, W., Xu, X., Lu, C., Pan, S., Chen, H., Hui, D., McNulty, S., Lockaby, G., Vance, E., 2012. Century-scale responses of ecosystem carbon storage and flux to multiple environmental changes in the Southern United States. Ecosystems 15 (4), 674–694. https://doi.org/10.1007/s10021-012-9539-x.
- Tian, H., Yang, Q., Najjar, R.G., Ren, W., Friedrichs, M.A.M., Hopkinson, C.S., Pan, S., 2015. Anthropogenic and climatic influences on carbon fluxes from eastern North America to the Atlantic Ocean: a process-based modeling study. J. Geophys. Res. Biogeosciences 120 (4), 757–772. https://doi.org/10.1002/jgrg.v120.410.1002/ 2014.IG002760
- Trenberth, K.E., Shea, D.J., 2005. Relationships between precipitation and surface temperature. Geophys. Res. Lett. 32.
- U.S. Geological Survey, 2001. National Water Information System data available on the World Wide Web (Water Data for the Nation), accessed [June 10, 2001], at URL [http://waterdata.usgs.gov/nwis/].
- van Vliet, M.T.H., Ludwig, F., Kabat, P., 2013. Global streamflow and thermal habitats of freshwater fishes under climate change. Clim. Change 121 (4), 739–754.
- van Vliet, M.T.H., Yearsley, J.R., Franssen, W.H.P., Ludwig, F., Haddeland, I., Lettenmaier, D.P., Kabat, P., 2012. Coupled daily streamflow and water temperature modelling in large river basins. Hydrol. Earth Syst. Sci. 16 (11), 4303–4321.
- Van Wijk, W.R., De Vries, D.A., 1963. Periodic temperature variations in a homogeneous soil. Phys. Plant Environ. 1, 103–143.
- Waisanen, P.J., Bliss, N.B., 2002. Changes in population and agricultural land in conterminous United States counties, 1790 to 1997. Global Biogeochem. Cycles 16.
- Wanders, N., Vliet, M.T.H., Wada, Y., Bierkens, M.F.P., Beek, L.P.H.(., 2019. High-Resolution Global Water Temperature Modeling. Water Resour. Res. 55 (4),
- Webb, B.W., Hannah, D.M., Moore, R.D., Brown, L.E., Nobilis, F., 2008. Recent advances in stream and river temperature research. Hydrol. Process. 22 (7), 902–918. https://doi.org/10.1002/ISSN)1099-108510.1002/hyp.v22:710.1002/hyp.6994.
- Wehrly, K.E., Brenden, T.O., Wang, L., 2009. A comparison of statistical approaches for predicting stream temperatures across heterogeneous landscapes. JAWRA J. Am. Water Resour. Assoc. 45, 986–997. https://doi.org/10.1111/j.1752-1688.2009.00341.x.
- Wu, H., Kimball, J.S., Elsner, M.M., Mantua, N., Adler, R.F., Stanford, J., 2012. Projected climate change impacts on the hydrology and temperature of Pacific Northwest rivers. Water Resour. Res. 48 (11) https://doi.org/10.1029/2012WR012082.
 Yang, Q., Tian, H., Li, X., Ren, W., Zhang, B., Zhang, X., Wolf, J., 2016. Spatiotemporal
- Yang, Q., Iian, H., Li, X., Ren, W., Zhang, B., Zhang, X., Wolf, J., 2016. Spatiotemporal patterns of livestock manure nutrient production in the conterminous United States from 1930 to 2012. Sci. Total Environ. 541, 1592–1602.
- Yao, Y., Tian, H., Pan, S., Najjar, R.G., Friedrichs, M.A.M., Bian, Z., Li, H.-Y., Hofmann, E. E., 2021. Riverine carbon cycling over the past century in the Mid-Atlantic region of the United States. J. Geophys. Res. Biogeosci. 126 (5) https://doi.org/10.1029/2020JG005968.
- Yao, Y., Tian, H., Shi, H., Pan, S., Xu, R., Pan, N., Canadell, J.G., 2020. Increased global nitrous oxide emissions from streams and rivers in the Anthropocene. Nat. Clim. Change 10 (2), 138–142.
- Yearsley, J., 2012. A grid-based approach for simulating stream temperature. Water Resour. Res. 48 (3) https://doi.org/10.1029/2011WR011515.